



Impact study of the wastewater treatment plant effluents on fluorescence of coastal zone water using fluorescence EEM-PARAFAC

Ibrahim El-Nahhal, Roland Redon, Michel Raynaud, Yasser El-Nahhal, Stéphane Mounier

► To cite this version:

Ibrahim El-Nahhal, Roland Redon, Michel Raynaud, Yasser El-Nahhal, Stéphane Mounier. Impact study of the wastewater treatment plant effluents on fluorescence of coastal zone water using fluorescence EEM-PARAFAC. Environmental Science and Pollution Research, inPress, <10.1007/s11356-020-08842-w>. <hal-02555075>

HAL Id: hal-02555075

<https://hal.science/hal-02555075v1>

Submitted on 27 Apr 2020

HAL is a multi-disciplinary open access archive for the deposit and dissemination of scientific research documents, whether they are published or not. The documents may come from teaching and research institutions in France or abroad, or from public or private research centers.

L'archive ouverte pluridisciplinaire **HAL**, est destinée au dépôt et à la diffusion de documents scientifiques de niveau recherche, publiés ou non, émanant des établissements d'enseignement et de recherche français ou étrangers, des laboratoires publics ou privés.



HAL Authorization

**Impact study of the wastewater treatment plant effluents on fluorescence of coastal zone
water using fluorescence EEM-PARAFAC.**

EL-Nahhal Ibrahim^{a*}, Redon Roland^a, Raynaud Michel^a, EL-Nahhal Yasser^b, Mounier Stéphane^a

^a Université de Toulon, Aix Marseille Univ, CNRS, IRD, MIO - CS 60584, 83041 TOULON
CEDEX 9, France

^b Department of Environmental and Earth Sciences, Faculty of Science, The Islamic
University-Gaza Palestinian Territory, P.O Box 108

*Corresponding author : elnahhal.i@gmail.com (I.Y.EL-Nahhal)

61
62
63
64
65 ABSTRACT : Human activity puts pressures on coastal zone altering dissolved organic matter
66
67 quality. No specific self-differentiating fluorescence signal of the anthropogenic DOM in the
68
69 coastal zone is found in the literature. Solar irradiation were conducted on mixed samples of
70
71 River water, sea water, wastewater treatment plant effluent. Excitation Emission Matrices of
72
73 Fluorescence were used to monitor the fate of wastewater treatment plant effluent. Multilinear
74
75 regression of CP/PARAFAC components contribution depending on mixing composition were
76
77 done and was excellent. Kinetics of decreasing contribution versus irradiation time were
78
79 investigated. Second order Kinetics were found for C1 and C2. Distinction between fluorescence
80
81 signal of endmembers was undoable. Wastewater treatment plant endmember after
82
83 photodegradation was highly predominant.
84
85
86
87
88

89
90 Keywords : Fluorescent Organic Matter, EEM-PARAFAC , multilinear regression,
91
92 photodegradation, Coastal zone
93
94
95

96 1. Introduction

97
98 Coastal zone is a transitional zone between the terrestrial and oceanic zones (Huguet et al.
99
100 2009) and mixing zone between marine/oceanic waters inputs and the freshwater riverine inputs
101
102 (Parlanti et al. 2000a). Dissolved organic matter (DOM) play an important role in physical,
103
104 chemical functioning of aquatic ecosystems (Hansell 2009) and biogeochemical processes
105
106 (Hansell & Carlson 2014a) and is a heterogenous mixture of organic compounds of both aromatic
107
108 and aliphatic nature (Hansell & Carlson 2014b). Chromophoric Dissolved Organic Matter
109
110 (CDOM) is a fraction of DOM which can interact with light (Coble 1996a; Coble 2007; Lei et al.
111
112 2018) and is ubiquitous in aquatic environmental media (Nelson & Siegel 2013) with a subgroup
113
114
115
116
117
118
119
120

fluorescing FDOM (Coble 1996b; Mostofa et al. 2012). DOM plays a key role in global carbon cycle (Hansell 2001) and is highly influenced by continental inputs (Fichot & Benner 2012; Yamashita et al. 2013) and by autochthonous sources (Romera-Castillo et al. 2011). Most of organic matter in the coastal zone is of terrestrial origin (Hedges et al. 1997; Parlanti et al. 2000b).

Human activity has contributed to increased inputs of terrestrial CDOM in aquatic ecosystems (Massicotte et al. 2017). Urbanization is increasing and expected to triple between 2000 and 2030 (Seto et al. 2012) with higher population density and migration to the coastal zone (Hugo 2011a; Hugo 2011b). In turn, it changes land cover, hence quality and quantity of DOM in rivers (Seto et al. 2012). Anthropogenic sources of organic matter vary from industrial (Carvalho et al. 2008), agricultural (Manninen et al. 2018), wastewater treatment plants effluents (Maizel & Remucal 2017), landfill leachates (Oloibiri et al. 2017). Moreover, it has been found (Williams et al. 2016) that anthropogenic influence on urban watersheds caused distinct DOM composition. However, contribution of anthropogenic signal of FDOM in coastal zone is not yet well defined and evaluated in the literature. Biogeochemistry of natural waters is impacted significantly by photo-reactivity of CDOM (Andrew et al. 2013; Lønborg et al. 2016) since photochemistry affects bioavailability of DOM (Moran & Zepp 1997; Oleinikova et al. 2017), microbial activity (Piccini et al. 2009) and production of DOM of different character (Zhu, Yang, et al. 2017).

Partial information can be extracted from global analytical techniques (DOC, TOC, BOD, etc...) due to complex composition of DOM. And these techniques are time consuming and require elaborated sample preparation. Optical properties of CDOM and FDOM provides a valuable tool in delineating DOM sources (Osburn et al. 2016a) and tracking DOM fluxes of

terrigenous origin into ocean (Osburn et al. 2016b) enables online or real-time monitoring in various media (Helms et al. 2013; Cohen et al. 2014). There are so many advantages of fluorescence spectroscopy which is useful, less time-consuming, inexpensive, precise qualitative and quantitative technique (Fellman et al. 2010; Zhu et al. 2014) used among varying scientific fields (Gao et al. 2017b). Excitation Emission Matrix fluorescence spectroscopy (EEM) has furthered scientific research in aquatic systems (Kim & Kim 2015; Dainard et al. 2015; Sgroi et al. 2017; Cheng et al. 2018). It enables characterization of optical properties of FDOM due to its high sensitivity, good selectivity and non-destruction of samples (Coble 1996c). Coupled with Canonical Polyadic / Parallel Factor Analysis (CP/PARAFAC) enables deconvolution of overlapping independent EEM spectra into distinct components (Stedmon & Bro 2008a). In addition, the use of this technique EEM/PARAFAC in tracing the DOM fractions which is cost-effective and rapid in chemistry and aquatic ecology fields is in fact a significant advance in those fields (Stedmon et al. 2003a).

To the best of our knowledge, there is no previously found pattern or specific self-distinguishing fluorescence signal of anthropogenic organic matter in the coastal zone. The present study is focussing on wastewater treatment plants effluent discharge in urban river systems. Laboratory endmember mixing experiments was conducted of river water, sea water and wastewater treatment plant, to define contributions after mixing and solar irradiation experiment. The present study is the first of its kind to develop and propose a multivariate linear regression for the prediction of FDOM signal and its photodegradation kinetic as a function of the mixing composition and solar exposure.

2. Material and methods

2.1 Sampling Sites

Gapeau river originates at Signes city (43° 17' 24" N, 5° 52' 59" E) and run till the sea at city of Hyères (43°06'42" N, 6°11'33" E) in southeastern part of France (figure 1) with a length of 34.4 km (Ollier 1972) and watershed of 544 km² (Ducros et al. 2018) with a pluvial regime. River water (RW) was sampled roughly 500 m before wastewater treatment plant which is located at (43°08'38.6"N 6°05'36.1"E) whereas wastewater treatment plant effluent (WW) was sampled at its output directly. Wastewater treatment plant of La Crau city has a daily volume of 0.17 m³/s. Sea water (SW) was sampled at the coastal area of Hyères city at roughly seven meters far from beach (43°06'10.4"N 6°10'38.3"E). Plastic bottle of one liter (cleaned with ethanol 100% and three times rinsed with 18.2 MΩ at 25 °C MilliQ water) was used in sampling.



Fig. 1. Locations of sampling sites in Southeastern France. RW , WW , SW are the points from left to right colored in red.

2.2. Materials of irradiation experiment

2.2.1. Filtration

RW , SW , WW samples were filtered using MilliPore filters (Type GNWP 0.20 μm , 47 mm diameter) and filtration kit pre-rinsed with acidified water (10% HNO_3). Filterates were put in a new one liter dark glass bottle (pre-rinsed with 10 % HNO_3 and 3 times with 18.2 $\text{M}\Omega\cdot\text{cm}$ at 25 $^\circ\text{C}$ MilliQ-water) and transferred to refrigerator at 4 $^\circ\text{C}$ in the dark. Filtrates were used for preparation of 15 mixtures. The measured pH for RW, WW ,SW were 7.4 ± 0.4 .

2.2.2. Preparation of mixtures

Fifteen 50 mL quartz vials were washed with reverse osmosis water then transferred to 10 % HNO_3 bath for 24 hours then rinsed three times with 18.2 $\text{M}\Omega\cdot\text{cm}$ at 25 $^\circ\text{C}$ Milli Q-water. Then burnt in oven at 450 $^\circ\text{C}$ for 24 hours to ensure the elimination of organic/inorganic carbon. Fifteen mixtures were fabricated. The exact mixing percentages for each mixture are summarized in table S1 in supplementary information SI. Percentages were taken by weight, assuming a density of 1.00, 1.00 and 1.025 for WW, RW and SW respectively. A serial number was given to the vial according to its corresponding mixture (table S1). Each vial was shaken gently by hand to insure homogeneity of mixtures.

2.2.3. Irradiation experiments

The mixtures were prepared in quartz vials which then were transferred on August 28th 2015 in the evening to the roof of laboratory MIO/Toulon University (43° 08' 11.2" N 6° 01' 16.7" E). These quartz vials were put at sufficient distances to insure receiving same solar irradiation conditions. The irradiation started on August 28th 2015 (Day zero) and finished on September 11th 2015 for a total of ten days of irradiation.

2.2.4. Solar irradiation/insolation measurement

Daily solar insolation data were measured on place in volts using photovoltaic cell (Solar Cell 9V/109 mA) for each day of irradiation. A mean irradiance of 2 343 volts per day was detected. During this period the irradiation is between 5 to 6 kWh.m⁻² corresponding to 39 mW.cm⁻² (www.meteofrance.com).

2.3. Excitation Emission Matrix EEM fluorescence spectroscopy

2.3.1. Irradiated water Sampling

Three mL aliquots from each 50 mL exposed quartz vial were sampled and transferred into 10x10 mm quartz cell at different irradiation times. EEMs of solar irradiation experiment sample were performed using fluorescence spectrophotometer (F4500, Hitachi). Ultrapure Perkin Elmer deionized water was measured to check spectrofluorimeter stability and measure daily the Raman peak intensity. Scan speed was set at 2,400 nm.min⁻¹. Emission spectra were collected at 5 nm

intervals between 220 and 420 nm, while excitation spectra were measured between 200 and 400 nm at 5 nm intervals. Slit widths for both excitation and emission wavelengths were set at 5 nm.

2.3.2. EEM Data processing

2.3.2.1. Raman measurement

Water Raman scans of Perkin Elmer blanks were measured for each irradiation day (from Aug. 28th to Sept. 11th 2015) using the same fluorescence spectrophotometer (F4500, Hitachi). Scans used an excitation wavelength of 350 nm whereas the emission intensities were measured from 350 nm to 650 nm with a step of 1 nm. Scan speed was 240 nm.mn⁻¹ with the same slit width of 5 nm on excitation and emission monochromators.

2.3.2.2. Raman Normalization

Each excitation emission matrix values corresponding to each mixture were normalized to the integrated Raman signal measured at the corresponding irradiation date. The integrated Raman signal was calculated by integration the area under the curve from 370 nm to 420 nm (Lawaetz & Stedmon 2009) and used for EEMs normalisation.

Spectral contribution of each CP/PARAFAC components to total EEM fluorescence was determined using CP/PARAFAC algorithm (Bro 1997; Stedmon & Markager 2005a). Finally, the 150 Raman-corrected EEMs were modelled using a MATLAB software (MathWorks R2015b) based on Nway toolbox and DOMFluor toolbox (Stedmon & Bro 2008b). Raman and Rayleigh scattering were removed according to Zepp method (Zepp et al. 2004). No inner filter correction was done as samples were in linearity domain. Nonnegativity constraints were applied for

CP/PARAFAC components for excitation and emission loadings. Accepted correct number of CP/PARAFAC components and model validation was taken according to evaluation of CONCORDIA score and split-half analysis. No outliers were found in the dataset and a three components model was validated. Once decomposition is done, for each mixture, contributions of each components were normalised to the maximum value in the whole EEM dataset, which is, in that work, the initial one before the start of solar irradiation for all experiments, according to the following equation :

$$C_i^{T_n} = \frac{c_i^{T_n}}{\max(c_i^{T_n})} \quad (\text{eq.1})$$

Where :

T_n is the n^{th} day of irradiation. $c_i^{T_n}$ is value of contribution of CP/PARAFAC component i and $C_i^{T_n}$ the normalised to the maximum contribution of CP/PARAFAC component i from 1 to 3 components.

2.4. Multi-linear regression

Considering f_{RW} , f_{SW} which are the percentage (w/w) of RW and SW in the quartz vial mixture respectively, a multi-linear regression was conducted for all f_{RW} , f_{SW} of a fixed CP/PARAFAC component i for each irradiation day T_n , considering the following general multilinear regression formula :

$$Y = a_0 + a_1.X_1 + a_2.X_2 + \dots + a_n.X_n \quad (\text{eq. 2})$$

2.4.1. Multilinear regression of three endmember

RW, SW and WW mixture is constrained by mass total sum of three content fraction that should be equal to 100 according to the following equation :

$$f_{SW} + f_{RW} + f_{WW} = 100 \quad (0 \leq f_i \leq 100) \quad (\text{eq.3})$$

Where f_{SW} , f_{RW} , f_{WW} are content fraction of SW, RW and WW in mass respectively. All percent fractions obviously positive and less than or equal to 100.

Then

$$f_{WW} = 100 - f_{SW} - f_{RW} \quad (\text{eq. 4})$$

By substituting in eq. 2 for f_{WW} where $n=3$, the different terms, the following equation can be obtained :

$$C_i^{Tn} = a_{i,0} + a_{i,1}.f_{SW} + a_{i,2}.f_{RW} + a_{i,3}.f_{WW} \quad (\text{eq.5})$$

Where C_i^{Tn} is normalised contribution of CP/PARAFAC component number i , and $a_{i,1}$, $a_{i,2}$, $a_{i,3}$ the respective partial contribution to this contribution by the three endmember SW, RW and WW. To simplify, C_i^{Tn} is replaced by C_i^* in the next equations

By substituting for f_{WW} by its expression in (eq.4) the following equations can be obtained :

$$C_i^* = a_{i,0} + a_{i,1}f_{SW} + a_{i,2}f_{RW} + a_{i,3}(100 - f_{SW} - f_{RW}) \quad (\text{eq.6})$$

$$C_i^* = a_{i,0} + a_{i,1}f_{SW} + a_{i,2}f_{RW} + a_{i,3}100 - a_{i,3}f_{SW} - a_{i,3}f_{RW} \quad (\text{eq.7})$$

By arranging similar terms together and taking the common factor, the following equation can be obtained :

$$C_i^* = (a_{i,0} + a_{i,3}100) + (a_{i,1} - a_{i,3})f_{SW} + (a_{i,2} - a_{i,3})f_{RW} \quad (\text{eq.8})$$

By giving a proper term for the constant and newly modified coefficients to account for f_{WW} term as shown :

$$A_{i,0}^{WW} = (a_{i,0} + a_{i,3}100) \quad A_{i,1}^{WW} = (a_{i,1} - a_{i,3}) \quad A_{i,2}^{WW} = (a_{i,2} - a_{i,3})$$

The final multilinear regression equation is obtained as a function of two content fractions of two endmembers :

$$C_i^* = A_{i,0}^{WW} + A_{i,1}^{WW}f_{SW} + A_{i,2}^{WW}f_{RW} \quad (\text{eq.9})$$

Where $A_{i,0}^{WW}$, $A_{i,1}^{WW}$ and $A_{i,2}^{WW}$ represent multilinear regression coefficients related to mixing equation when f_{WW} is expressed in terms of content fraction of the other two endmembers (f_{RW} and f_{SW}). Any circular permutation can not yield the $a_{i,*}$ coefficients independently.

$A_{i,0}^{WW}$ is the constant in the multilinear regression equation which contains information about WW effect in the multilinear regression, $A_{i,1}^{WW}$ is the coefficient of content fraction of SW endmember which not only represent its effect but also the effect of the wastewater treatment plant effluent WW, $A_{i,2}^{WW}$ is the coefficient of content fraction of RW endmember which not only represent its effect but also the effect of WW. Determination of $A_{i,0}^{WW}$, $A_{i,1}^{WW}$ and $A_{i,2}^{WW}$ was done for each exposition day.

2.5. Kinetics

The measured irradiation in volts was used as a proxy for photodegradation reaction time . The determination of the kinetic order of the multilinear regression parameters/coefficients for all T_n was conducted. These multilinear regression are expressed mathematically as a function of volts :

$$\begin{aligned} A_{i,0}^{WW}(V) \\ A_{i,1}^{WW}(V) \\ A_{i,2}^{WW}(V) \end{aligned} \tag{eq.10}$$

Where V is received solar irradiation in Volts (V) at each day T_n . CP/PARAFAC contribution during irradiation experiment can be expressed as a function of content fraction of two endmember depending on V , which enable kinetic study:

$$C_i^*(V) = A_{i,0}^{WW}(V) + A_{i,1}^{WW}(V) \cdot f_{SW} + A_{i,2}^{WW}(V) \cdot f_{RW} \quad (\text{ep.11})$$

The zeroth, 1st, 2nd and 3rd order kinetics were calculated and compared to find out the most linear model which fits the data (Wright 2004).

3. Results and Discussion

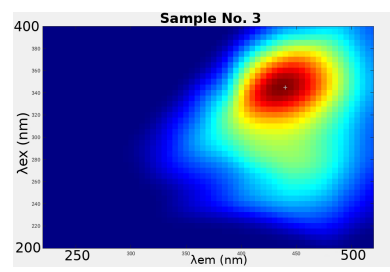
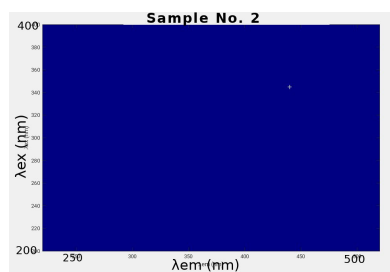
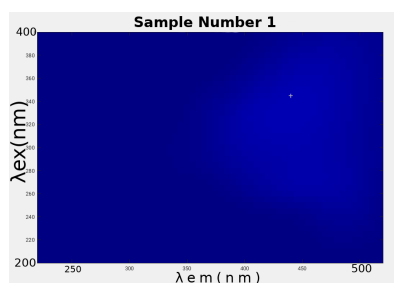
3.1. EEMs Results

Figure 2. shows the excitation emission matrices EEM of fluorescence for the samples numbers 1, 2, 3, 13, 14, 15 which are described in table 2. These EEMs are shown after the removal of Rayleigh and Raman scattering and Raman normalization.

Sample No. :1

Sample No. : 2

Sample No. : 3



Sample No. : 13

Sample No. : 15

Sample No. : 14

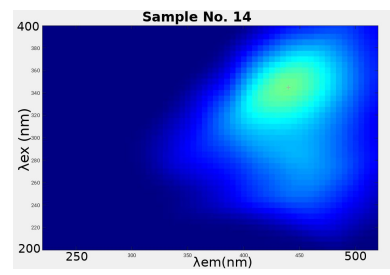
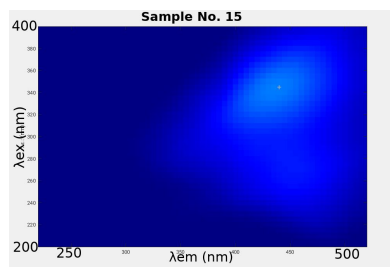
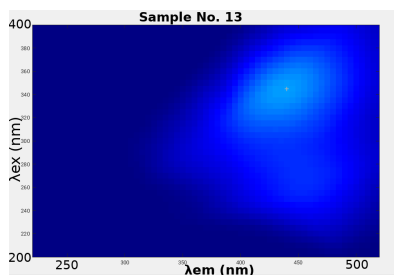
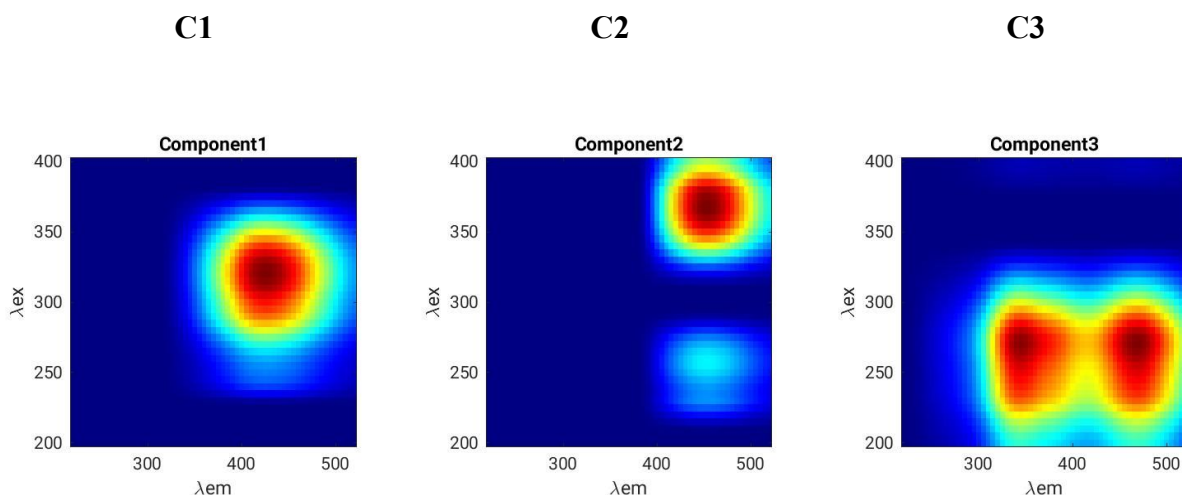


Fig. 2. The excitation emission matrices of Samples number 1 , 2 ,3, 13 , 14 and 15 whose composition is (100,0,0), (0,100,0) ,(0,0,100), (50,0,0), (0,50,0) and (0,0,50) respectively (table S1)

Split-half analysis was conducted for three subsets of the EEM-dataset which asserted the non-existence "finding" of any protein-like fluorescent signal. That's because the CP/PARAFAC algorithm doesn't capture what's already not there.

3.2. CP/PARAFAC decomposition results

CORCONDIA analysis showed drop down between four components and five, from near 70 % to less than or around 30 % which surpasses acceptable threshold of 60% where as it showed a value of 80.75 % for three components, indicating that a three-factor model was appropriate. The split-half analysis confirm this three components model. Spectral contour plots of components and their corresponding loadings for both the excitation and the emission wavelengths are shown in figure 3.



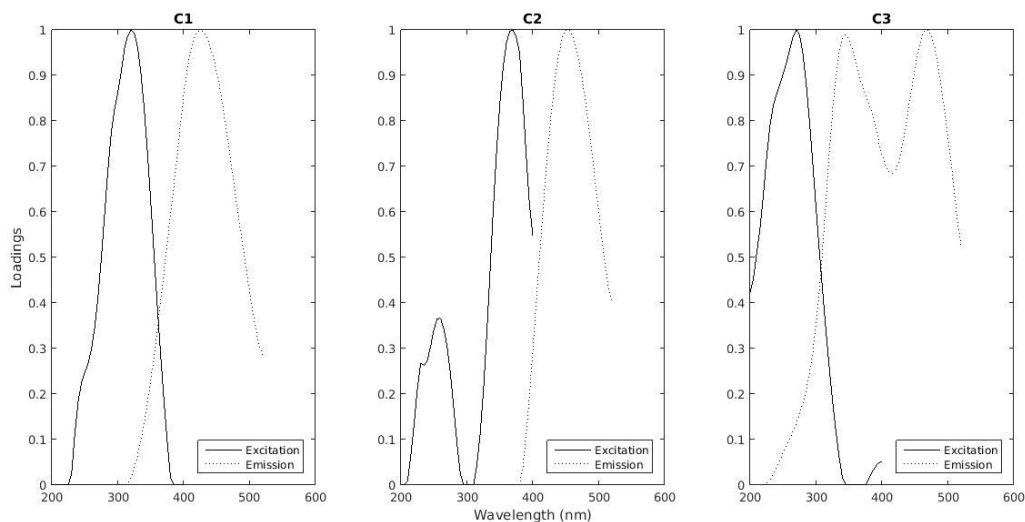


Fig. 3. Contour plots of CP/PARAFAC components found in EEM dataset. Spectral loadings of excitation and emission wavelengths of the three identified CP/PARAFAC in the present study.

Description of excitation and emission pairs of main peak positions for CP/PARAFAC components are summarized in Table 1 and compared to previously identified components and peaks in the literature.

Table 1

Descriptions of CP/PARAFAC components and comparison with literature

Component	$\lambda_{EX}/\lambda_{EM}$ (nm)	Description and references in literature
Component C1	320/425	Component 4 (Stedmon et al. 2003b) : terrestrially derived organic matter Peak C (Coble 1996d; Coble et al. 1998) : visible humic-like Component 2 (Yamashita et al. 2008a) : terrestrial humic-like Component 4 (Yamashita et al. 2008b)
Component C2	370/455	Component 3 (Stedmon et al. 2003c) Component G3 (Murphy et al. 2011a) Component 3 (Li et al. 2014a) Component 7 (Osburn et al. 2016a) Component 5 (Bagthoth et al. 2011) Component 1 (Zhu et al. 2017a) Humic-Like Component 3 (Yamashita et al. 2008c) : Humic-like component
Component C3	270/(340) 470	Peak T : Tryptophan like fluorescence (Coble 1996d) Q2 (Cory & McKnight 2005) Small resemblance to C6 (Zhou et al. 2013) which was Oil-related, degradation product

Based on maximum peak position, these three components have been previously identified (Table 1). C1, showed an excitation maximum at 320 nm and an emission maximum at 425 nm and a range of excitation emission wavelengths (Ex=300-350 nm, Em=400-450 nm). Previous studies have associated this component to UVA humic-like fluorescent CP/PARAFAC component and Peak C (Coble 2007) and peak “ ∞ ” (Parlanti et al. 2000c; Sierra et al. 2005). It was previously found from terrestrial, anthropogenic, agricultural sources (Stedmon et al. 2003d; Stedmon & Markager 2005b). C2 component showed an excitation maximum at 370 nm and an emission maximum at 455 nm and a range of excitation emission wavelengths (Ex=340-400 nm, Em= 400-500 nm). In addition, spectra of C2 resembles spectra of component “G3” which has $Ex_{max}=350$ nm, $Em_{max}=428$ nm in (Murphy et al. 2011b) who have attributed it to wastewater or nutrient enrichment tracer. This component has also been identified as humic-like component, similar to “C3” (Li et al. 2014b) which had two excitation maxima (at 250, 350 nm) corresponding to the same emission maxima (at 440 nm). Furthermore, C2 has very similar spectra to “C7” from recycled water studies, which included samples of wastewater, treated water, gray water (Osburn et al. 2016b). C3, showed an excitation maximum at 270 nm and an emission maximum at 340 nm and 470 nm which is bimodal in emission. It’s range of excitation emission wavelengths is Ex=200-300 nm, Em=300-500 nm. The 1st peak (270/340 nm) is near the tryptophan-like peak (Coble 1996e). This component could be protein-like component but it resembles noise.

3.3. Multivariate Linear Regression Parameters

Numerical values of multilinear regression coefficients (eq. 9) for each CP/PARAFAC component C1, C2 and C3 are the following for time zero, i.e. Aug. 28th 2015.

For

$$C1 = 100.45 - 0.99 * f_{SW} - 0.93 * f_{RW} \text{ with coefficient of determination } r^2 \text{ value of } 0.99$$

$$C2 = 98.67 - 0.97 * f_{SW} - 0.92 * f_{RW} \text{ with } r^2 \text{ value of } 0.99$$

$$C3 = 72.84 - 0.66 * f_{SW} - 0.64 * f_{RW} \text{ with } r^2 \text{ value of } 0.84$$

From the above substituted equations, it can be seen that the correlation coefficient is greater than 0.95 for C1 and C2 indicating multilinear regression is excellent. Values of the intercept are always greater than values of coefficients of f_{SW} and f_{RW} by two orders of magnitude. These values of the parameters/coefficients of the multilinear regression are calculated after the Raman unit corrections of the EEM-dataset. Knowing that values of the intercept account for effect of f_{WW} on contribution of CP/PARAFAC component, these results show that contribution of CP/PARAFAC component decreases with increasing f_{SW} or f_{RW} . Indeed, all of coefficients f_{SW} , f_{RW} have negative sign. As a consequence, it can be observed that for $f_{SW}=100$ or $f_{RW}=100$, contributions are weak compared to the $f_{WW}=100$, i.e. $f_{SW}=f_{RW}=0$. These indicated that most of fluorescence contributions are due to WW endmember considering the blank fluorescence $a_{i,0}$ as negligible. Considering that WW is the principal contributor to the all components contribution, there is no specific end member response for SW and RW in these mixtures.

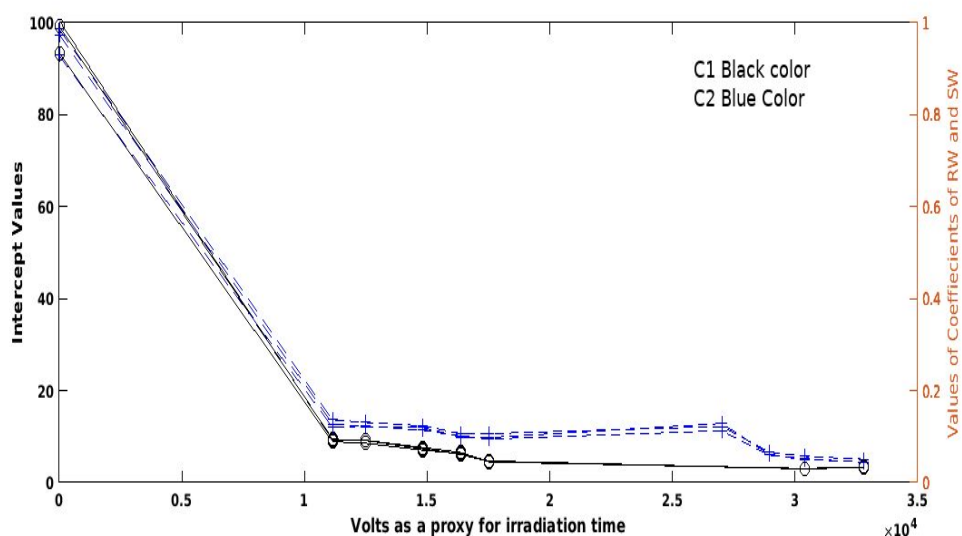


Fig. 4. The variation with irradiation time (volts as proxy for time) of the parameters of multilinear regression (Intercept , absolute values of f_{RW} coefficient, absolute values of f_{SW} coefficient) for C1 and C2 .

The intercept and the coefficients of f_{RW} and f_{SW} of CP/PARAFAC C1 (shown in black) has a faster degradation rate than their counterparts of C2 (shown in blue) as shown in figure 4. which in agreements with the values of the kinetic rate constants as shown in table 6 .

3.4. Determination of kinetic decay coefficient and its kinetic order

The irradiation experiment showed continuous decrease of fluorescence signal with irradiation time. No stable signal or significant fluorescence increase was observed like in other works (; Song et al. 2015; Zhu et al. 2017b). Integrated rate law linear equations of zeroth, 1st, 2nd, and 3rd kinetic order were investigated for each coefficient $A_{i,0}^{WW}$, $A_{i,1}^{WW}$ and $A_{i,3}^{WW}$ to determine kinetics of photodegradation for each multilinear regression parameter. Kinetic order was chosen according to the best coefficient of determination according to kinetic integrated order law,

selecting linear correlation coefficient which must be greater than the threshold 0.75 after eliminating outliers (Wright 2004). Results are presented in table 2 for kinetic order, and kinetic constant are presented in table 3. It was found that all kinetics are 2nd order and are in agreement with a previous work (Yang et al. 2014). Long term photodegradation of fluorescent organic matter is a bimolecular reaction probably involving excited organic matter and organic matter itself. Other work assumed first order kinetic under solar simulated irradiation (Wu et al. 2016) but experiment were done during 12h and under 2.80 mW.cm⁻² (visible) and 70.00 mW.cm⁻², corresponding to the starting point of present irradiation experiment that could be assumed as pseudo-first order kinetic. On the same time, Hee et al 2018 didn't find variation with a 4,2 mW.cm⁻², during 10 hours of exposition.

Table 2

Kinetic order of coefficients of multilinear regression for each CP/PARAFAC with its corresponding r^2 of 2nd order kinetics to the right. "NA" means that correlation coefficient for 2nd order rate was less than 0.75, and was dismissed.

C1						C2						C3		
$A^{ww}_{1,0}$	r^2	$A^{ww}_{1,1}$	r^2	$A^{ww}_{1,2}$	r^2	$A^{ww}_{2,1}$	r^2	$A^{ww}_{2,1}$	r^2	A^{ww}_2	r^2	$A^{ww}_{3,1}$	$A^{ww}_{3,2}$	$A^{ww}_{3,3}$
<i>interpt</i>		(f_{sw})		(f_{rw})		<i>interpt</i>		(f_{sw})		2		<i>interpt</i>	(f_{sw})	(f_{rw})
										(f_{rw})				
2	0.94	2	0.95	2	0.96	2	0.83	2	0.78	2	0.82	NA	NA	NA

Table 2 clearly shows that the kinetic order of photodegradation reaction for each parameter of the multi-linear regression for CP/PARAFAC components C1 and C2 are second-order kinetics and the corresponding coefficient of determination r^2 is greater than 0.75. For the third

CP/PARAFAC component C3 , no order could be found since this component is noise-like component (table 3) and it was neglected from the analysis.

Table 3

Kinetic constant for coefficients of multilinear regression for each CP/PARAFAC component.

Values in parenthesis are standard deviation for kinetic constant. All values should be multiplied by 10^6 . NA : Not Available

	C1	C2	C3
$A^{WW}_{*,0}$	9.68(1.00)	4.85(0.78)	NA
<i>interpt</i>			
$A^{WW}_{*,1}$	-987.35(92.31)	-542.80(101.97)	NA
(f_{SW})			
$A^{WW}_{*,2}$	-977.67(83.84)	-552.56(91.70)	NA
(f_{RW})			

Values of kinetic constant for intercept for both C1 and C2 are smaller than those values of kinetic constant for $A^{WW}_{*,1}$ which is coefficient of f_{SW} and $A^{WW}_{*,2}$ which is coefficient of f_{RW} (table 3). This result could be interpreted as follows: C1 and C2 contributions of RW and SW are more sensitive to photodegradation than WW which in turn decays approximately 100 times slower under irradiation suggesting its dominance in the residual fluorescence of both C1 and C2 after long term irradiation. Hence even if there is no specific endmember CP/PARAFAC

contribution, it exist a photosensitivity difference between WW and RW or SW. Under long irradiation, WW contribution is more resilient and refractory to photodegradation. This difference of behavior depending on endmember mixing was already observed between terrestrial and autochthonous organic matter (Zhu et al. 2017c). Small differences were also observed on reclaimed water using fluorescence matrix regional integration between humic-like and protein-like under high irradiation (Wu et al. 2016). Therefore, it can be said that wastewater treatment plant fluorophores are somehow similar to natural fluorophores but more refractory to photodegradation. Anthropogenic dissolved organic matter, in the present study, remains and constitute the greatest contribution of CP/PARAFAC components along irradiation process. Fluorescence signal going to the coastal zone should mainly come from WW endmember.

Comparing C1 versus C2 degradation kinetic, it was observed that humic-like FDOM is more reactive than protein-like FDOM (Yang et al. 2014). However, results above demonstrated that it's not so simple. CP/PARAFAC components are constituted by several types of FDOM fluorophores which behave differently depending on their origin and photosensitivity.

(Timko et al. 2015) found increasing rates of photochemical fluorescent DOM loss with increasing pH studied thru measurements on the EEMs not between the parameters of multilinear regression between CP/PARAFAC components and mixing composition . However, pH of RW , SW and WW were constant ($pH=7.4 \pm 0.4$) in this study suggesting no effect of pH in the results of the kinetic analysis

4. Conclusions

In this study, fluorescent conservative behaviour and natural solar changes on three endmember mixing laboratory experiment were investigated leading to the following conclusions

(1) Multilinear regression model for contribution of CP/PARAFAC components is excellent and could be done for the three endmembers in addition to being able to study the kinetic evolution.

(2) Two of the three fluorescence CP/PARAFAC extracted component (C1 “terrestrial humic like” and C2 “humic-like of longer wavelength”) showed a second order photodegradation toward the irradiation process whatever the endmember mixture composition.

(3) Search for specific self-distinguishing fluorescence signal or signature for river water, wastewater treatment plants and sea water couldn’t be done in this work, which could be attributed to the complexity of the anthropogenic and natural dissolved organic matter.

(4) The fluorescence signal of wastewater treatment plant effluent is predominant in the studied coastal zone, according to the results of photodegradation kinetic constant which favour anthropogenically-impacted organic matter contribution (100 times less sensitive to photobleaching). However, its exact contribution couldn’t be found due to inability to calculate or find its coefficient $a_{i,3}$ in the multilinear regression model independently.

(5) In human impacted coastal zone, residual fluorescent organic matter comes from wastewater treatment plant effluent, and no specific fluorescence signal either from sea water or from wastewater treatment plant effluent could be detected near the coast.

Acknowledgements

The authors acknowledge Erasmus Mundus/Hermes program for financial support of present work; Météo-France for providing irradiation data. Christian Martino is thanked for participating in sampling campaigns. Two anonymous reviewers are thanked for their comments which ameliorated the quality of this article.

Declarations of interest none

Appendix A. Supplementary Information (SI)

Supplementary Information to this article can be found in the Supplementary Information (SI) file

References

1. Andrew, A.A. et al., 2013. Chromophoric dissolved organic matter (CDOM) in the Equatorial Atlantic Ocean: Optical properties and their relation to CDOM structure and source. *Marine chemistry*, 148, pp.33–43. Available at: <http://dx.doi.org/10.1016/j.marchem.2012.11.001>.
2. Baghoth, S.A., Sharma, S.K. & Amy, G.L., 2011. Tracking natural organic matter (NOM) in a drinking water treatment plant using fluorescence excitation–emission matrices and PARAFAC. *Water research*, 45(2), pp.797–809. Available at: <http://dx.doi.org/10.1016/j.watres.2010.09.005>.
3. Bro, R., 1997. PARAFAC. Tutorial and applications. *Chemometrics and Intelligent Laboratory Systems*, 38(2), pp.149–171. Available at: [http://dx.doi.org/10.1016/s0169-7439\(97\)00032-4](http://dx.doi.org/10.1016/s0169-7439(97)00032-4).
4. Carvalho, S.I.M. et al., 2008. Effects of solar radiation on the fluorescence properties and

- molecular weight of fulvic acids from pulp mill effluents. *Chemosphere*, 71(8), pp.1539–1546. Available at: <http://dx.doi.org/10.1016/j.chemosphere.2007.11.046>.
5. Cheng, C. et al., 2018. Novel insights into variation of dissolved organic matter during textile wastewater treatment by fluorescence excitation emission matrix. *Chemical engineering journal*, 335, pp.13–21. Available at: <http://dx.doi.org/10.1016/j.cej.2017.10.059>.
 6. Coble, P.G., 1996a. Characterization of marine and terrestrial DOM in seawater using excitation-emission matrix spectroscopy. *Marine chemistry*, 51(4), pp.325–346. Available at: [http://dx.doi.org/10.1016/0304-4203\(95\)00062-3](http://dx.doi.org/10.1016/0304-4203(95)00062-3).
 7. Coble, P.G., 1996b. Characterization of marine and terrestrial DOM in seawater using excitation-emission matrix spectroscopy. *Marine chemistry*, 51(4), pp.325–346. Available at: [http://dx.doi.org/10.1016/0304-4203\(95\)00062-3](http://dx.doi.org/10.1016/0304-4203(95)00062-3).
 8. Coble, P.G., 1996c. Characterization of marine and terrestrial DOM in seawater using excitation-emission matrix spectroscopy. *Marine chemistry*, 51(4), pp.325–346. Available at: [http://dx.doi.org/10.1016/0304-4203\(95\)00062-3](http://dx.doi.org/10.1016/0304-4203(95)00062-3).
 9. Coble, P.G., 1996d. Characterization of marine and terrestrial DOM in seawater using excitation-emission matrix spectroscopy. *Marine chemistry*, 51(4), pp.325–346. Available at: [http://dx.doi.org/10.1016/0304-4203\(95\)00062-3](http://dx.doi.org/10.1016/0304-4203(95)00062-3).
 10. Coble, P.G., 1996e. Characterization of marine and terrestrial DOM in seawater using excitation-emission matrix spectroscopy. *Marine chemistry*, 51(4), pp.325–346. Available at: [http://dx.doi.org/10.1016/0304-4203\(95\)00062-3](http://dx.doi.org/10.1016/0304-4203(95)00062-3).
 11. Coble, P.G., 2007. Marine optical biogeochemistry: the chemistry of ocean color. *Chemical reviews*, 107(2), pp.402–418. Available at: <http://dx.doi.org/10.1021/cr050350+>.

12. Coble, P.G., Del Castillo, C.E. & Avril, B., 1998. Distribution and optical properties of CDOM in the Arabian Sea during the 1995 Southwest Monsoon. *Deep-sea research. Part II, Topical studies in oceanography*, 45(10-11), pp.2195–2223. Available at: [http://dx.doi.org/10.1016/s0967-0645\(98\)00068-x](http://dx.doi.org/10.1016/s0967-0645(98)00068-x).
13. Cohen, E., Levy, G.J. & Borisover, M., 2014. Fluorescent components of organic matter in wastewater: efficacy and selectivity of the water treatment. *Water research*, 55, pp.323–334. Available at: <http://dx.doi.org/10.1016/j.watres.2014.02.040>.
14. Cory, R.M. & McKnight, D.M., 2005. Fluorescence Spectroscopy Reveals Ubiquitous Presence of Oxidized and Reduced Quinones in Dissolved Organic Matter. *Environmental science & technology*, 39(21), pp.8142–8149. Available at: <http://dx.doi.org/10.1021/es0506962>.
15. Dainard, P.G. et al., 2015. Photobleaching of fluorescent dissolved organic matter in Beaufort Sea and North Atlantic Subtropical Gyre. *Marine chemistry*, 177, pp.630–637. Available at: <http://dx.doi.org/10.1016/j.marchem.2015.10.004>.
16. Ducros, L. et al., 2018. Tritium in river waters from French Mediterranean catchments: Background levels and variability. *The Science of the total environment*, 612, pp.672–682. Available at: <http://dx.doi.org/10.1016/j.scitotenv.2017.08.026>.
17. Fellman, J.B., Hood, E. & Spencer, R.G.M., 2010. Fluorescence spectroscopy opens new windows into dissolved organic matter dynamics in freshwater ecosystems: A review. *Limnology and oceanography*, 55(6), pp.2452–2462. Available at: <http://dx.doi.org/10.4319/lo.2010.55.6.2452>.
18. Fichot, C.G. & Benner, R., 2012. The spectral slope coefficient of chromophoric dissolved organic matter (S₂₇₅₋₂₉₅) as a tracer of terrigenous dissolved organic carbon in river-influenced ocean margins. *Limnology and oceanography*, 57(5), pp.1453–1466.

Available at: <http://dx.doi.org/10.4319/lo.2012.57.5.1453>.

19. Gao, J. et al., 2017b. Spectral characteristics of dissolved organic matter in various agricultural soils throughout China. *Chemosphere*, 176, pp.108–116. Available at: <http://dx.doi.org/10.1016/j.chemosphere.2017.02.104>.
20. Hansell, D., 2001. Marine Dissolved Organic Matter and the Carbon Cycle. *Oceanography*, 14(4), pp.41–49. Available at: <http://dx.doi.org/10.5670/oceanog.2001.05>.
21. Hansell, D.A., 2009. Dissolved organic carbon in the carbon cycle of the Indian Ocean. In *Geophysical Monograph Series*. pp. 217–230. Available at: <http://dx.doi.org/10.1029/2007gm000684>.
22. Hansell, D.A. & Carlson, C.A., 2014a. *Biogeochemistry of Marine Dissolved Organic Matter*, Academic Press. Available at: <https://market.android.com/details?id=book-7iKOAwAAQBAJ>.
23. Hansell, D.A. & Carlson, C.A., 2014b. *Biogeochemistry of Marine Dissolved Organic Matter*, Academic Press. Available at: <https://market.android.com/details?id=book-7iKOAwAAQBAJ>.
24. Hedges, J.I., Keil, R.G. & Benner, R., 1997. What happens to terrestrial organic matter in the ocean? *Organic geochemistry*, 27(5-6), pp.195–212. Available at: [http://dx.doi.org/10.1016/s0146-6380\(97\)00066-1](http://dx.doi.org/10.1016/s0146-6380(97)00066-1).
25. Helms, J.R. et al., 2013. Photochemical bleaching of oceanic dissolved organic matter and its effect on absorption spectral slope and fluorescence. *Marine chemistry*, 155, pp.81–91. Available at: <http://dx.doi.org/10.1016/j.marchem.2013.05.015>.
26. Hugo, G., 2011a. Future demographic change and its interactions with migration and climate change. *Global environmental change: human and policy dimensions*, 21,

- pp.S21–S33. Available at: <http://dx.doi.org/10.1016/j.gloenvcha.2011.09.008>.
27. Hugo, G., 2011b. Future demographic change and its interactions with migration and climate change. *Global environmental change: human and policy dimensions*, 21, pp.S21–S33. Available at: <http://dx.doi.org/10.1016/j.gloenvcha.2011.09.008>.
28. Huguet, A. et al., 2009. Properties of fluorescent dissolved organic matter in the Gironde Estuary. *Organic geochemistry*, 40(6), pp.706–719. Available at: <http://dx.doi.org/10.1016/j.orggeochem.2009.03.002>.
29. Kim, J. & Kim, G., 2015. Importance of colored dissolved organic matter (CDOM) inputs from the deep sea to the euphotic zone: Results from the East (Japan) Sea. *Marine chemistry*, 169, pp.33–40. Available at: <http://dx.doi.org/10.1016/j.marchem.2014.12.010>.
30. Lawaetz, A.J. & Stedmon, C.A., 2009. Fluorescence intensity calibration using the Raman scatter peak of water. *Applied spectroscopy*, 63(8), pp.936–940. Available at: <http://dx.doi.org/10.1366/000370209788964548>.
31. Lei, X., Pan, J. & Devlin, A.T., 2018. Mixing behavior of chromophoric dissolved organic matter in the Pearl River Estuary in spring. *Continental shelf research*, 154, pp.46–54. Available at: <http://dx.doi.org/10.1016/j.csr.2018.01.004>.
32. Li, W.-T. et al., 2014a. Characterization of dissolved organic matter in municipal wastewater using fluorescence PARAFAC analysis and chromatography multi-excitation/emission scan: a comparative study. *Environmental science & technology*, 48(5), pp.2603–2609. Available at: <http://dx.doi.org/10.1021/es404624q>.
33. Li, W.-T. et al., 2014b. Characterization of dissolved organic matter in municipal wastewater using fluorescence PARAFAC analysis and chromatography multi-excitation/emission scan: a comparative study. *Environmental science & technology*, 48(5), pp.2603–2609. Available at: <http://dx.doi.org/10.1021/es404624q>.

34. Lønborg, C. et al., 2016. Photochemical alteration of dissolved organic matter and the subsequent effects on bacterial carbon cycling and diversity. *FEMS microbiology ecology*, 92(5), p.fiw048. Available at: <http://dx.doi.org/10.1093/femsec/fiw048>.
35. Maizel, A.C. & Remucal, C.K., 2017. The effect of advanced secondary municipal wastewater treatment on the molecular composition of dissolved organic matter. *Water research*, 122, pp.42–52. Available at: <http://dx.doi.org/10.1016/j.watres.2017.05.055>.
36. Manninen, N. et al., 2018. Effects of agricultural land use on dissolved organic carbon and nitrogen in surface runoff and subsurface drainage. *The Science of the total environment*, 618, pp.1519–1528. Available at: <http://dx.doi.org/10.1016/j.scitotenv.2017.09.319>.
37. Massicotte, P. et al., 2017. Global distribution of dissolved organic matter along the aquatic continuum: Across rivers, lakes and oceans. *The Science of the total environment*, 609, pp.180–191. Available at: <http://dx.doi.org/10.1016/j.scitotenv.2017.07.076>.
38. Moran, M.A. & Zepp, R.G., 1997. Role of photoreactions in the formation of biologically labile compounds from dissolved organic matter. *Limnology and oceanography*, 42(6), pp.1307–1316. Available at: <http://dx.doi.org/10.4319/lo.1997.42.6.1307>.
39. Mostofa, K.M.G. et al., 2012. Fluorescent Dissolved Organic Matter in Natural Waters. In *Environmental Science and Engineering*. pp. 429–559. Available at: http://dx.doi.org/10.1007/978-3-642-32223-5_6.
40. Murphy, K.R. et al., 2011a. Organic Matter Fluorescence in Municipal Water Recycling Schemes: Toward a Unified PARAFAC Model. *Environmental science & technology*, 45(7), pp.2909–2916. Available at: <http://dx.doi.org/10.1021/es103015e>.
41. Murphy, K.R. et al., 2011b. Organic Matter Fluorescence in Municipal Water Recycling Schemes: Toward a Unified PARAFAC Model. *Environmental science & technology*,

- 45(7), pp.2909–2916. Available at: <http://dx.doi.org/10.1021/es103015e>.
42. Nelson, N.B. & Siegel, D.A., 2013. The global distribution and dynamics of chromophoric dissolved organic matter. *Annual review of marine science*, 5, pp.447–476. Available at: <http://dx.doi.org/10.1146/annurev-marine-120710-100751>.
43. Oleinikova, O.V. et al., 2017. Dissolved organic matter degradation by sunlight coagulates organo-mineral colloids and produces low-molecular weight fraction of metals in boreal humic waters. *Geochimica et cosmochimica acta*, 211, pp.97–114. Available at: <http://dx.doi.org/10.1016/j.gca.2017.05.023>.
44. Ollier, J., 1972. Contribution à l'étude physico-chimique de quelques sources du bassin versant du Gapeau (Var). *Bulletin mensuel de la Societe linneenne de Lyon*, 41(3), pp.41–48. Available at: <http://dx.doi.org/10.3406/linly.1972.9979>.
45. Oloibiri, V. et al., 2017. Characterisation of landfill leachate by EEM-PARAFAC-SOM during physical-chemical treatment by coagulation-flocculation, activated carbon adsorption and ion exchange. *Chemosphere*, 186, pp.873–883. Available at: <http://dx.doi.org/10.1016/j.chemosphere.2017.08.035>.
46. Osburn, C.L., Boyd, T.J., et al., 2016a. Optical Proxies for Terrestrial Dissolved Organic Matter in Estuaries and Coastal Waters. *Frontiers in Marine Science*, 2. Available at: <http://dx.doi.org/10.3389/fmars.2015.00127>.
47. Osburn, C.L., Boyd, T.J., et al., 2016b. Optical Proxies for Terrestrial Dissolved Organic Matter in Estuaries and Coastal Waters. *Frontiers in Marine Science*, 2. Available at: <http://dx.doi.org/10.3389/fmars.2015.00127>.
48. Osburn, C.L., Handsel, L.T., et al., 2016a. Predicting Sources of Dissolved Organic Nitrogen to an Estuary from an Agro-Urban Coastal Watershed. *Environmental science & technology*, 50(16), pp.8473–8484. Available at:

- <http://dx.doi.org/10.1021/acs.est.6b00053>.
49. Osburn, C.L., Handsel, L.T., et al., 2016b. Predicting Sources of Dissolved Organic Nitrogen to an Estuary from an Agro-Urban Coastal Watershed. *Environmental science & technology*, 50(16), pp.8473–8484. Available at: <http://dx.doi.org/10.1021/acs.est.6b00053>.
50. Parlanti, E. et al., 2000a. Dissolved organic matter fluorescence spectroscopy as a tool to estimate biological activity in a coastal zone submitted to anthropogenic inputs. *Organic geochemistry*, 31(12), pp.1765–1781. Available at: [http://dx.doi.org/10.1016/s0146-6380\(00\)00124-8](http://dx.doi.org/10.1016/s0146-6380(00)00124-8).
51. Parlanti, E. et al., 2000b. Dissolved organic matter fluorescence spectroscopy as a tool to estimate biological activity in a coastal zone submitted to anthropogenic inputs. *Organic geochemistry*, 31(12), pp.1765–1781. Available at: [http://dx.doi.org/10.1016/s0146-6380\(00\)00124-8](http://dx.doi.org/10.1016/s0146-6380(00)00124-8).
52. Parlanti, E. et al., 2000c. Dissolved organic matter fluorescence spectroscopy as a tool to estimate biological activity in a coastal zone submitted to anthropogenic inputs. *Organic geochemistry*, 31(12), pp.1765–1781. Available at: [http://dx.doi.org/10.1016/s0146-6380\(00\)00124-8](http://dx.doi.org/10.1016/s0146-6380(00)00124-8).
53. Piccini, C. et al., 2009. Alteration of chromophoric dissolved organic matter by solar UV radiation causes rapid changes in bacterial community composition. *Photochemical & photobiological sciences: Official journal of the European Photochemistry Association and the European Society for Photobiology*, 8(9), pp.1321–1328. Available at: <http://dx.doi.org/10.1039/b905040j>.
54. Romera-Castillo, C. et al., 2011. Net production and consumption of fluorescent colored dissolved organic matter by natural bacterial assemblages growing on marine

- phytoplankton exudates. *Applied and environmental microbiology*, 77(21), pp.7490–7498. Available at: <http://dx.doi.org/10.1128/AEM.00200-11>.
55. Seto, K.C., Güneralp, B. & Hutyra, L.R., 2012. Global forecasts of urban expansion to 2030 and direct impacts on biodiversity and carbon pools. *Proceedings of the National Academy of Sciences of the United States of America*, 109(40), pp.16083–16088. Available at: <http://dx.doi.org/10.1073/pnas.1211658109>.
56. Sgroi, M. et al., 2017. Monitoring the Behavior of Emerging Contaminants in Wastewater-Impacted Rivers Based on the Use of Fluorescence Excitation Emission Matrixes (EEM). *Environmental science & technology*, 51(8), pp.4306–4316. Available at: <http://dx.doi.org/10.1021/acs.est.6b05785>.
57. Sierra, M.M.D. et al., 2005. Fluorescence fingerprint of fulvic and humic acids from varied origins as viewed by single-scan and excitation/emission matrix techniques. *Chemosphere*, 58(6), pp.715–733. Available at: <http://dx.doi.org/10.1016/j.chemosphere.2004.09.038>.
58. Song, W. et al., 2015. Effects of irradiation and pH on fluorescence properties and flocculation of extracellular polymeric substances from the cyanobacterium *Chroococcus minutus*. *Colloids and surfaces. B, Biointerfaces*, 128, pp.115–118. Available at: <http://dx.doi.org/10.1016/j.colsurfb.2015.02.017>.
59. Stedmon, C.A. & Bro, R., 2008a. Characterizing dissolved organic matter fluorescence with parallel factor analysis: a tutorial. *Limnology and oceanography, methods / ASLO*, 6(11), pp.572–579. Available at: <http://dx.doi.org/10.4319/lom.2008.6.572b>.
60. Stedmon, C.A. & Bro, R., 2008b. Characterizing dissolved organic matter fluorescence with parallel factor analysis: a tutorial. *Limnology and oceanography, methods / ASLO*, 6(11), pp.572–579. Available at: <http://dx.doi.org/10.4319/lom.2008.6.572b>.

61. Stedmon, C.A. & Markager, S., 2005a. Resolving the variability in dissolved organic matter fluorescence in a temperate estuary and its catchment using PARAFAC analysis. *Limnology and oceanography*, 50(2), pp.686–697. Available at: <http://dx.doi.org/10.4319/lo.2005.50.2.0686>.
62. Stedmon, C.A. & Markager, S., 2005b. Resolving the variability in dissolved organic matter fluorescence in a temperate estuary and its catchment using PARAFAC analysis. *Limnology and oceanography*, 50(2), pp.686–697. Available at: <http://dx.doi.org/10.4319/lo.2005.50.2.0686>.
63. Stedmon, C.A., Markager, S. & Bro, R., 2003a. Tracing dissolved organic matter in aquatic environments using a new approach to fluorescence spectroscopy. *Marine chemistry*, 82(3-4), pp.239–254. Available at: [http://dx.doi.org/10.1016/s0304-4203\(03\)00072-0](http://dx.doi.org/10.1016/s0304-4203(03)00072-0).
64. Stedmon, C.A., Markager, S. & Bro, R., 2003b. Tracing dissolved organic matter in aquatic environments using a new approach to fluorescence spectroscopy. *Marine chemistry*, 82(3-4), pp.239–254. Available at: [http://dx.doi.org/10.1016/s0304-4203\(03\)00072-0](http://dx.doi.org/10.1016/s0304-4203(03)00072-0).
65. Stedmon, C.A., Markager, S. & Bro, R., 2003c. Tracing dissolved organic matter in aquatic environments using a new approach to fluorescence spectroscopy. *Marine chemistry*, 82(3-4), pp.239–254. Available at: [http://dx.doi.org/10.1016/s0304-4203\(03\)00072-0](http://dx.doi.org/10.1016/s0304-4203(03)00072-0).
66. Stedmon, C.A., Markager, S. & Bro, R., 2003d. Tracing dissolved organic matter in aquatic environments using a new approach to fluorescence spectroscopy. *Marine chemistry*, 82(3-4), pp.239–254. Available at: [http://dx.doi.org/10.1016/s0304-4203\(03\)00072-0](http://dx.doi.org/10.1016/s0304-4203(03)00072-0).

67. Timko, S.A., Gonsior, M. & Cooper, W.J., 2015. Influence of pH on fluorescent dissolved organic matter photo-degradation. *Water research*, 85, pp.266–274. Available at: <http://dx.doi.org/10.1016/j.watres.2015.08.047>.
68. Williams, C.J. et al., 2016. Human activities cause distinct dissolved organic matter composition across freshwater ecosystems. *Global change biology*, 22(2), pp.613–626. Available at: <http://dx.doi.org/10.1111/gcb.13094>.
69. Wright, M.R., 2004. *Introduction to Chemical Kinetics*, Wiley. Available at: <https://market.android.com/details?id=book-pZQn1RYcFuYC>, 455 pp.
70. Wu, Q. et al., 2016. Removal of fluorescence and ultraviolet absorbance of dissolved organic matter in reclaimed water by solar light. *Journal of environmental sciences*, 43, pp.118–127. Available at: <http://dx.doi.org/10.1016/j.jes.2015.08.021>.
71. Yamashita, Y. et al., 2008a. Assessing the dynamics of dissolved organic matter (DOM) in coastal environments by excitation emission matrix fluorescence and parallel factor analysis (EEM-PARAFAC). *Limnology and oceanography*, 53(5), pp.1900–1908. Available at: <http://dx.doi.org/10.4319/lo.2008.53.5.1900>.
72. Yamashita, Y. et al., 2008b. Assessing the dynamics of dissolved organic matter (DOM) in coastal environments by excitation emission matrix fluorescence and parallel factor analysis (EEM-PARAFAC). *Limnology and oceanography*, 53(5), pp.1900–1908. Available at: <http://dx.doi.org/10.4319/lo.2008.53.5.1900>.
73. Yamashita, Y. et al., 2008c. Assessing the dynamics of dissolved organic matter (DOM) in coastal environments by excitation emission matrix fluorescence and parallel factor analysis (EEM-PARAFAC). *Limnology and oceanography*, 53(5), pp.1900–1908. Available at: <http://dx.doi.org/10.4319/lo.2008.53.5.1900>.
74. Yamashita, Y., Boyer, J.N. & Jaffé, R., 2013. Evaluating the distribution of terrestrial

- dissolved organic matter in a complex coastal ecosystem using fluorescence spectroscopy. *Continental shelf research*, 66, pp.136–144. Available at: <http://dx.doi.org/10.1016/j.csr.2013.06.010>.
75. Yang, X. et al., 2014. Sunlight-induced changes in chromophores and fluorophores of wastewater-derived organic matter in receiving waters--the role of salinity. *Water research*, 62, pp.281–292. Available at: <http://dx.doi.org/10.1016/j.watres.2014.05.050>.
76. Zepp, R.G., Sheldon, W.M. & Moran, M.A., 2004. Dissolved organic fluorophores in southeastern US coastal waters: correction method for eliminating Rayleigh and Raman scattering peaks in excitation–emission matrices. *Marine chemistry*, 89(1-4), pp.15–36. Available at: <http://dx.doi.org/10.1016/j.marchem.2004.02.006>.
77. Zhou, Z. et al., 2013. Characterization of oil components from the Deepwater Horizon oil spill in the Gulf of Mexico using fluorescence EEM and PARAFAC techniques. *Marine chemistry*, 148, pp.10–21. Available at: <http://dx.doi.org/10.1016/j.marchem.2012.10.003>.
78. Zhu, G. et al., 2014. DOM removal by flocculation process: Fluorescence excitation–emission matrix spectroscopy (EEMs) characterization. *Desalination*, 346, pp.38–45. Available at: <http://dx.doi.org/10.1016/j.desal.2014.04.031>.
79. Zhu, W.-Z., Yang, G.-P. & Zhang, H.-H., 2017. Photochemical behavior of dissolved and colloidal organic matter in estuarine and oceanic waters. *The Science of the total environment*, 607-608, pp.214–224. Available at: <http://dx.doi.org/10.1016/j.scitotenv.2017.06.163>.
80. Zhu, W.-Z., Zhang, J. & Yang, G.-P., 2017a. Mixing behavior and photobleaching of chromophoric dissolved organic matter in the Changjiang River estuary and the adjacent East China Sea. *Estuarine, coastal and shelf science*. Available at: <http://linkinghub.elsevier.com/retrieve/pii/S0272771417302743>.

- 2221
2222
2223 81. Zhu, W.-Z., Zhang, J. & Yang, G.-P., 2017b. Mixing behavior and photobleaching of
2224
2225 chromophoric dissolved organic matter in the Changjiang River estuary and the adjacent
2226
2227 East China Sea. *Estuarine, coastal and shelf science*. Available at:
2228
2229 <http://linkinghub.elsevier.com/retrieve/pii/S0272771417302743>.
2230
2231
2232 82. Zhu, W.-Z., Zhang, J. & Yang, G.-P., 2017c. Mixing behavior and photobleaching of
2233
2234 chromophoric dissolved organic matter in the Changjiang River estuary and the adjacent
2235
2236 East China Sea. *Estuarine, coastal and shelf science*. Available at:
2237
2238 <http://linkinghub.elsevier.com/retrieve/pii/S0272771417302743>.
2239
2240
2241 83. Zhu, W.-Z., Zhang, J., & Yang, G.-P. (2017). Mixing behavior and photobleaching of
2242
2243 chromophoric dissolved organic matter in the Changjiang River estuary and the adjacent
2244
2245 East China Sea. *Estuarine, Coastal and Shelf Science*.
2246
2247 <https://doi.org/10.1016/j.ecss.2017.07.019>
2248
2249
2250
2251
2252
2253
2254
2255
2256
2257
2258
2259
2260
2261
2262
2263
2264
2265
2266
2267
2268
2269
2270
2271
2272
2273
2274
2275
2276
2277
2278
2279
2280

Table S1

Percentages by weight of RW , SW ,WW used in the preparation of fifteen mixtures in Quartz vials for mixing and solar irradiation experiment

Sample Serial Number															
Endmember	1	2	3	4	5	6	7	8	9	10	11	12	13	14	15
f_{RW}	100	0	0	75	50	25	75	50	25	0	0	0	50	25	25
f_{SW}	0	100	0	25	50	75	0	0	0	25	50	75	25	25	50
f_{WW}	0	0	100	0	0	0	25	50	75	75	50	25	25	50	25